Оптический журнал

Оптическое приборостроение

UDC 535-1

DOI:10.17586/1023-5086-2018-85-09-74-83

Создание зеркал с малым шагом ступенек для инфракрасного статического фурье-спектрометра и анализ ошибок их плоскостности

© 2018 г. Min Zhang, Jingqiu Liang, Zhongzhu Liang, Jinguang Lv, Yuxin Qin, and Weibiao Wang

Предложен инфракрасный статический фурье-спектрометр, использующий ступенчатые зеркала с малым шагом. Поскольку такие зеркала являются базовым компонентом спектрометра, их параметры существенно влияют на работу устройства. Для изготовления ступенчатого зеркала с большой апертурой и субмикронным шагом ступенек предложен способ многократного последовательного нанесения слоев с уменьшением на 50% толщины каждого последующего слоя, что позволяет контролировать точность, целостность и идентичность высот ступенек. Изготовлены зеркала, содержащие 32 ступеньки высотой 625 нм. Результаты тестирования показали наличие деформаций ступенек, вызванных воздействием сжимающих напряжений. Эти деформации могут привести к изменению разности длины оптического пути и повлиять на восстановление спектра. Моделированием и расчетным путем получены данные о влиянии плоскостности ступенек на результаты восстановления спектра. Напряжения падают с увеличением толщины подложки зеркал. Выполнены эксперименты, в процессе которых с помощью предложенного инфракрасного статического фурье-спектрометра получены спектрограммы ацетонитрила путем соответствующей обработки интерферограмм.

Ключевые слова: *спектроскопия, инфракрасный фурье-спектрометр, анализ спектра, ступенчатое зеркало с малым шагом.*

Fabrication and flatness error analysis of low-stepped mirror in static Fourier transform infrared spectrometer

© 2018 г. Min Zhang*, **; Jingqiu Liang*; Zhongzhu Liang*; Jinguang Lv*; Yuxin Qin*, and Weibiao Wang*

**State Key Laboratory of Applied Optics, Changchun Institute of Optics, Fine Mechanics and Physics, Chinese Academy of Sciences, Changchun, Jilin, 130033, China*

***University of Chinese Academy of Sciences, Beijing 100049, China*

E-mail: liangjq@ciomp.ac.cn, liangzz@ciomp.ac.cn

Submitted 06.03.2018

In this study, we propose a Fourier transform infrared spectrometer based on stepped mirrors, which realize static. As the core component of the spectrometer, the low-stepped mirror's structural parameters significantly affect the instrument performance. In order to successfully fabricate a low-stepped mirror with large area and sub-micron height, we propose a method involving multiple depositions accompanied by a 50% reduction in thickness at every iteration, which can precisely control the accuracy, consistency, and uniformity of the step height. After that, we fabricate a low-stepped mirror consisting of 32 stages and with a step height of 625 nm. Through theoretical calculation and simulation analysis, the influence of the step's flatness error on the recovery spectrum is obtained. By increasing the substrate thickness of the stepped mirror, we can reduce the stress of the thin film. We perform experiments using the low-stepped mirror. The low-stepped

mirror was incorporated into the Fourier transform infrared spectrometer, and we performed experiments to obtain the spectrum of acetonitrile liquid. The spectrogram of the acetonitrile is obtained by processing the interferogram.

Keywords: *spectroscopy, Fourier transform infrared spectrometer, low-stepped mirror, spectrum analysis.*

OCIS codes: *300.6190, 300.6300, 230.4000*

1. INTRODUCTION

Spectrometers are widely used in medicine, physics, aerospace, agriculture and other fields [1]. Compared with other types of spectrometer, the Fourier transform spectrometer (FTS) has good potential in spectral analysis with advantages including having multi-channel, high radiation flux and precise wave number [2]. In addition to the ability to detect solid, liquid, and gas samples, an FTS can also analyse organic and inorganic matter, polymers and coordination compounds, not only qualitatively but also quantitatively [3]. With respect to its advantages, it has been widely used in many fields. An FTS based on a Michelson interferometer with the two plane mirrors replaced by two stepped mirrors was proposed by Möller [4, 5] and later studied by others [6–9]. Such a static FTS is able to obtain the static configuration and microminiaturize the instrument, as well as to realize real-time detection and online monitoring. A Fourier transform infrared spectrometer based on stepped mirrors (SMFTIRS) was proposed by Jingqiu Liang et al., and the diffraction effect, design and fabrication of tall-stepped mirrors, spectrum reconstruction, were studied [10–14]. The optical path differences (OPDs) are discretized by two vertical stepped mirrors with different heights. As the key component of SMFTIRS, the low-stepped mirror has the characteristics of large area and submicron height. Height consistency, surface flatness, and the height accuracy of the low-stepped mirror affect the spectral sampling interval, resolution, and noise directly. When the fabrication error is sufficiently large, the interferogram is reversed and incorrect spectral information is obtained. Therefore, it is important for achieving high-precision fabrication and error analysis of the device.

In this paper, a method of 'multiple depositions accompanied by a 50% reduction in film thickness at every iteration' is proposed, which can precisely control the accuracy, consistency, and uniformity of the step height using coating technology. To solve the problem of step-surface deformation caused by the compressive stress produced in the process, theoretical calculations and simulations were carried out to analyse the influence of the step-flatness error of the stepped mirror on the recovery spectrum. The relationship between the substrate thickness and the step-flatness error is obtained through experiments. A low-stepped mirror with a thickness of 5 mm was fabricated. Finally, an SMFTIRS is assembled and an experiment is carried out to obtain the spectrum curve of acetonitrile.

2. PRINCIPLE OF SMFTIRS

The simplified configuration of a static SMFTIRS is shown in Fig. 1. It comprises a light source, collimating system, sample compartment, beam splitter, two stepped mirrors, expansion system, and detector arrays. Light emitted from the light source propagates through the sample cell and collimating system, and then becomes a parallel beam to reach the beam splitter. The parallel beam is split by the beam splitter into two coherent lights, after which it then reaches the tall- and low-stepped mirror, which are vertical. They interfere when the beams return to the beam splitter. The array of OPDs is imaged by the detector. Then, the spectrum is obtained using the Fourier transform of the interferogram.

The SMFTIRS uses two vertical stepped mirrors instead of two classical plane mirrors, which are used in a Michelson interferometer. A spatial array of OPDs is obtained using vertical stepped mirrors. We considered the highest step of the stepped mirror as the first step, and the two mirrors have N steps. $\delta(m, n)$ is the OPD between the m^{th} step of the low-stepped mirror and the n^{th} step of the tall-stepped

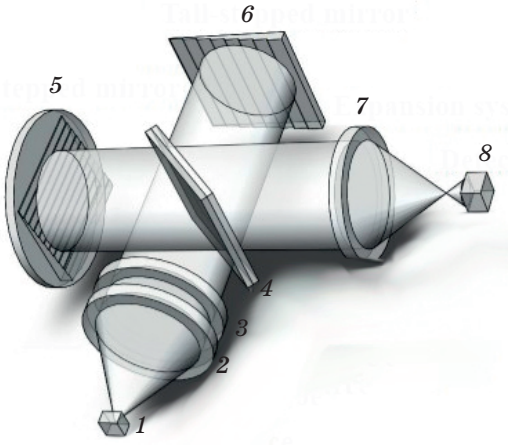

Fig. 1. Simplified configuration of a static SMFTIRS. *1* — light source, *2* — collimating system, *3* — sample compartment, *4* — beam splitter, *5* — low-stepped mirror, *6* — tall- stepped mirror, *7* — expansion system, *8* — detector.

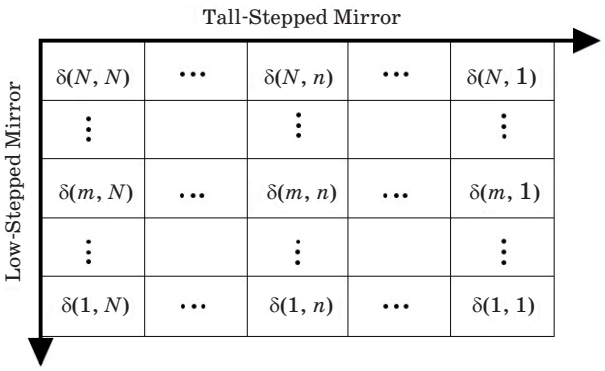

Fig. 2. Array showing distribution of OPDs.

mirror. Therefore, the OPD arrays at the detector can be set as it is shown in Fig. 2. Each row and column correspond to all sampling points which belong to the sub-mirror of the low- and tall-stepped mirror respectively. The arrow indicates the direction of the step height increase. The expression of the interference intensity is

$$I(\delta) = \int_{-\infty}^{\infty} B(\nu)\cos(2\pi\nu\delta)d\nu, \qquad (1)$$

where $I(\delta)$ is the interference intensity, $B(\nu)$ is the spectrum, δ is the OPD and ν is the spatial frequency, which is the reciprocal of the wavelength.

The two-dimensional interference image is expanded into a one-dimensional (1D) interference sequence, and the spectral information is obtained by the Fourier transform as follows:

$$B(\nu) = \int_{-\infty}^{\infty} I(\delta)\cos(2\pi\nu\delta)d\delta. \qquad (2)$$

3. DESIGN AND FABRICATION OF LOW-STEPPED MIRROR

3.1. Design of low-stepped mirror

The two mirrors are arranged into a stair-case pattern, one with lower steps, and the other with taller steps. Apart from reducing the size and mass of the instrument, these two stepped mirrors are also highly reliable and can be used repeatedly. As shown in Fig. 3, the step height of the low-stepped mirror is d. To verify the OPD's continuity, one step height of the tall-stepped mirror must be equal to the total height of the steps of low-stepped mirror, i.e. the height of the tall steps is Nd. This leads to a sampling interval of $\Delta = 2d$. Then, the OPD between the m^{th} step of the low-stepped mirror and the n^{th} step of the tall-stepped mirror can be expressed as

$$\delta(m,n) = 2(nNd - md) = 2d(Nn - m). \qquad (3)$$

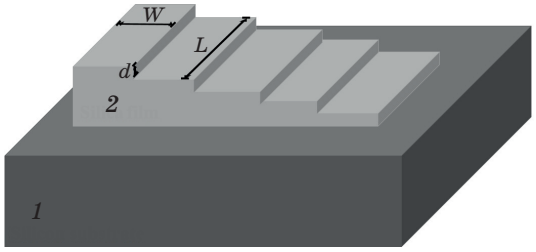

Fig. 3. Sketch of low-stepped mirror. *1* — silicon substrate, *2* — silica film.

According to the Nyquist–Shannon criterion, the sampling frequency must be greater than or equal to twice the maximum frequency of the signal being measured; therefore, the sampling interval is less than half of the minimum wavelength. For an operational wavelength ranging from 3.2 to 5 μm, the sampling interval is less than 1.6 μm. Then, one step height of the low-stepped mirror is smaller than 0.8 μm. Considering the effects of the spectrum resolution and diffraction, the width and height of the low-stepped mirror are 1 mm and 0.625 μm respectively. The maximum OPD, which is expressed as $\text{OPD}_{\max}$, should be greater than or equal to the inverse of the spectral resolution according to the discrete Fourier transform theory. To ensure that the spectral resolution is 8 cm^{-1}, $\text{OPD}_{\max}$ should be larger than 1250 μm. As $\text{OPD}_{\max} = 2N^2h$, the sampling points N^2 should be greater than 1000. In our system, we chose the number of steps to be 32, which can generate 1024 sample points with different OPDs.

3.2. Fabrication method of low-stepped mirror

Considering the structural characteristics and precision requirements of the low-stepped mirror, we propose a method of multiple depositions to fabricate the low-stepped mirror. Electron beam evaporation coating technology was applied to the manufacturing process. An ultraviolet positive-type photoresist AZ P4620 (AZ Electronic Materials, Japan) was chosen as the photoresist, and a double-sided polished monocrystalline silicon wafer was chosen as the substrate in the experiment. The process flow is shown in Fig. 4, and the details are explained as follows. (a) Cleaning the silicon wafer and spin-coating the photoresist. The thickness of the photoresist should be greater than that of the silica films to ensure that it works as a mask during the coating process. Before exposure, the sample was prebaked on a hotplate to remove the solvent in the photoresist, increasing the adhesion between the photoresist and the substrate. (b) Patterning the photoresist using a mask aligner and developing the sample using an AZ 400K solution. (c) Silica films with a thickness of 10 μm were deposited on silicon wafers with a mask via EBE. (d) After evaporation, the residual photoresist was

removed by soaking in the acetone bath until there was no trace of photoresist residue, and then, the two-step structure was obtained. The low-stepped mirror with 32 steps was fabricated by repeating steps (a) to (d). It should be noted that the film thickness and width is halved gradually as the coating times increase.

Using the above method, we fabricated a low-stepped mirror with 32 steps. The results show that the film thickness accuracy and the uniformity of each layer remain constant. However, the step is deformed, which can cause a change in the OPDs and affect the reconstruction of the spectrum during the manufacture of the low-stepped mirror. Stress is caused by several factors, such as imperfections in the structure of the substrate, the existence of surface morphology, lattice mismatches between the film and substrate, and differences in the thermal-expansion coefficients of the film and substrate.

Two kinds of stress exist during the coating process, namely, compressive stress and tensile stress. As shown in Fig. 5, stresses developed in films can

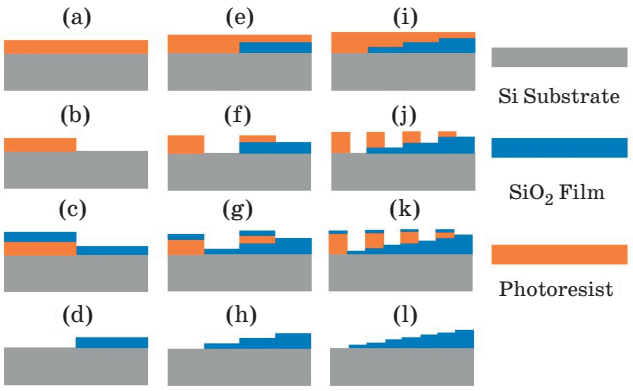

Fig. 4. Manufacture process of low-stepped mirror.

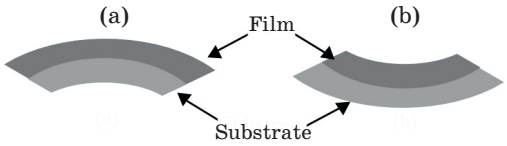

Fig. 5. (a) Compressive stress, (b) tensile stress.

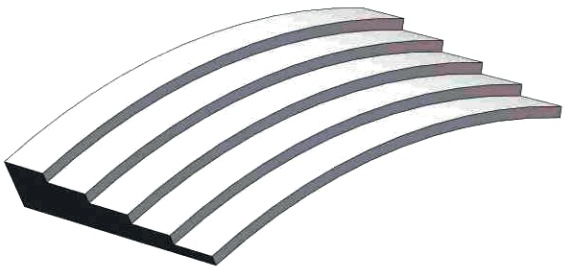

Fig. 6. Low-stepped mirror with deformation.

lead to film delamination and blistering in the case of compression, while they can lead to cracking and peeling in the case of tension [15]. The test results show that the step surfaces are bearing compressive stress during the process of making stepped mirrors, and a bend occurs along the direction of the sub-mirror, as shown in Fig. 6. The influence of the step surface's flatness error on the recovery spectrum is analysed by making theoretical calculations and simulations as follows.

4. FLATNESS ERROR ANALYSIS OF LOW-STEPPED MIRROR

4.1. Theoretical calculation of surface flatness error

When the surface of the stepped mirror is bent, the OPD between the tall-stepped mirror and low-stepped mirror is changed. Then, the OPD expression after deformation is

$$\delta'(m,n) = 2(Nn - m)d + \alpha(m,n), \tag{4}$$

where $\delta'(m, n)$ is the OPD between the m^{th} step of the low-stepped mirror and the n^{th} step of the tall-stepped mirror after deformation. $\alpha(m, n)$ is the additional OPD between the m^{th} low step and the n^{th} tall step. The OPD array when the step mirror is deformed is shown in Fig. 7.

We assume that the deformation of the 32 steps of the low-stepped mirror is the same, so the additional OPDs in each column in Fig. 7 are equal. Then, $\alpha(m, n)$ can be expressed as a function of $\alpha(\delta)$. The reconstructed spectrum is expressed as

$$B'(\nu) = \int_{-\infty}^{\infty} I'(\delta)\cos(2\pi\nu\delta)d\delta = \\ = \int_{-\infty}^{\infty}\int_{-\infty}^{\infty} B(\tau)\cos\left[2\pi\tau(\delta + \alpha(\delta)\right]\cos(2\pi\nu\delta)d\tau d\delta, \tag{5}$$

where $I'(\delta)$ is the interference intensity when the step is deformed, and $B'(\nu)$ is the spectrum when the step is deformed.

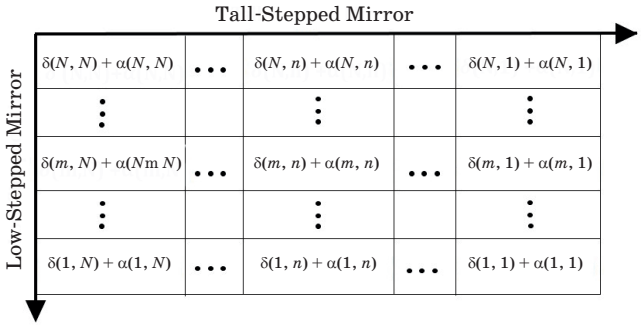

Fig. 7. The OPDs sequence when the low-stepped mirror deformed.

When the bending radius of the step surface is large, the additional OPDs between the adjacent steps of the tall-stepped mirror can be approximately considered as linear, and is represented by h.

$$\alpha(\delta)=\begin{cases}-2(N-1)h & 0<\delta\le 2Nd-2d\\ \cdots & \\ -h & N^2d-2Nd-2d<\delta\le N^2d-2d\\ -h & N^2d-2d<\delta\le N^2d+2Nd-2d\\ \cdots & \\ -(N-1)h & 2N^2d-2Nd-2d<\delta\le 2N^2d-2d\end{cases}. \quad (6)$$

Then, the recovery spectrum is

$$\begin{aligned}B'(\nu)=\Bigg|&\sum_{p=0}^{N/2-1}\int_{-\infty}^{\infty}B(\tau)\frac{\sin[2\pi Nd(\nu-\tau)]}{\pi(\nu-\tau)}\times\\ &\times\exp[-i2\pi[\nu-\tau](Nd-d+2pNd)+\\ &+i2\pi\tau(-(N-1)Kd+2pKd)]d\tau+\\ &+\sum_{q=0}^{N/2-1}\int_{-\infty}^{\infty}B(\tau)\frac{\sin[2\pi Nd(\nu-\tau)]}{\pi(\nu-\tau)}\times\\ &\times\exp[-i2\pi[\nu-\tau](Nd+N^2d-d+2qNd)+\\ &+i2\pi\tau(-Kd-2qKd)]\,d\tau\Bigg|,\end{aligned} \quad (7)$$

where the value of K is equal to the ratio of h to the step height d, which can describe the flatness error of the stepped mirror.

When the light source is monochromatic light,

$$\begin{aligned}B'(\nu)=\Bigg|&\left(\frac{\sin[2\pi Nd(\nu-\nu_0)]}{\pi(\nu-\nu_0)}\times\right.\\ &\times\frac{\sin[\pi(\nu-\nu_0)N^2d-\pi\nu_0Nkd]}{\sin[2\pi(\nu-\nu_0)Nd-2\pi\nu_0kd]}\times\\ &\times\exp\left[i\left(-\pi(\nu-\nu_0)N^2d-k\pi\nu_0Nd\right)\right]+\\ &+\frac{\sin[\pi(\nu-\nu_0)N^2d+\pi\nu_0Nkd]}{\sin[2\pi(\nu-\nu_0)Nd+2\pi\nu_0kd]}\times\\ &\left.\times\exp\left[i\left(-3\pi(\nu-\nu_0)N^2d-k\pi\nu_0Nd\right)\right]\right)\Bigg|\end{aligned} \quad (8)$$

by considering

$$\begin{aligned}&\sum_{p=0}^{2^n-1}\exp[i(p\alpha+\beta)]=\\ &=\exp\left[i(\beta+\frac{2^n-1}{2}\alpha)\right]\prod_{l=1}^{n}2\cos(2^{l-2}\alpha).\end{aligned} \quad (9)$$

When $K=0$, the ideal spectrum can be expressed as

$$B(\nu)=\frac{\sin\left(2\pi(\nu-\nu_0)N^2d\right)}{\pi(\nu-\nu_0)}. \quad (10)$$

From the above formula, we obtain the following conclusions:

(1) When $K=0$, the equation for $B'(\nu)$ is equal to the equation for $B(\nu)$.

(2) When $K\neq 0$, the value of $B'(\nu)$ at $\nu=\nu_0\pm 1/(2Nd)$ is not equal to 0, so the spectrum curve is broadened and the resolution is decreased.

(3) When $K\neq 0$, the intensity of the recovery spectrum will change with the error. When the error is serious, the shape of the main peak of the recovery spectrum will become different, which will lead to the peak position's shift and cause a drift of the spectral curve.

(4) When $\alpha_2(\delta)=\alpha_1(\delta)+C$, the function $B_2'(\nu)=B_1'(\nu)\exp(i2\pi\nu_0C)$ is established, where $|B_2'(\nu)|$ is equal to $|B_1'(\nu)|$. Thus, it will not affect the monochromatic light recovery spectrum when there is a tiny displacement of the stepped mirror in the optical-axis direction. This is an advantage of the static instrument which could not be realized by time-modulated FTS.

4.2. Simulation experiments of surface flatness error

To further discuss the influence of the step-flatness error on the spectrum, we simulate the static SMFTIRS using the simulation software, and monochromatic light is used as an example. The interferograms obtained from the detector are expanded into 1D OPD sequences in order. Then, the DC component is removed (the default value is 0.5 in ASAP), and the Fourier transform is performed. As shown in Fig. 8, the recovery spectra at different K values when the wavelength is 3.2, 4, and 5 μm is obtained. (a–c), (d–f), (g–j) and (k–m) show the spectral curves when K is 0.05, 0.1, 0.12, and 0.15 respectively. The curves *1* are obtained by the simulation software, and the curves *2* are the ideal spectral curves. The results of the calculation by Eq. (8) coincided with the result of simulation software, indicating that Eq. (8) correctly describes the spectrum of the step deformed.

When $K=0.05$, there is no deviation in the peak position for all wavelengths. When $K=0.1$, the width of the spectrum is broadened and the peak position of the spectral curve is shifted with a wavelength of 3.2 μm, and there is no deviation in the peak positions of 4 and 5 μm. When $K=0.12$, spectral curves of 3.2 and 4 μm appear in the double peak, and the peak position is shifted, while there is no deviation in the peak position of 5 μm. When $K=0.15$, the spectrum line for the whole wavelength band (3.2–5 μm) is distorted. With the increase of K, the peak position of the spectrum is shifted. For the same K, the degeneration of the spectrum curve for a short wavelength is larger than that of a long wavelength.

The full width at half maximum (FWHM) can describe the spectral resolution of SMFTIRS. Fig. 9 describes the FWHM for different values of K at

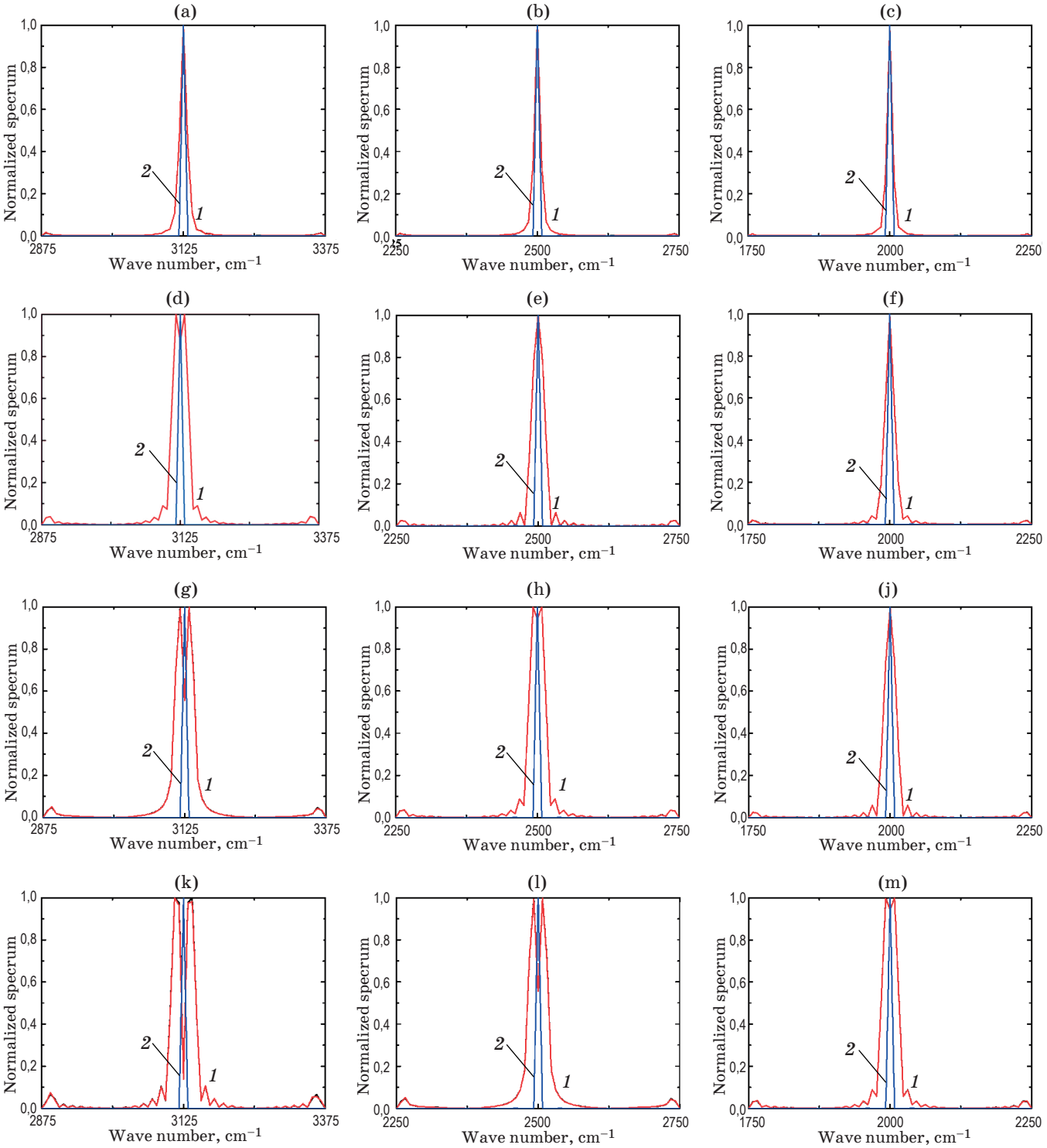

Fig. 8. Spectral curves at different K values (a–c — $K = 0.05$, d–f — $K = 0.1$, g–j — $K = 0.12$, k–m — $K = 0.15$) when the wavelength 3.2 (a, d, g, k), 4 (b, e, h, l), and 5 (c, f, j, m) μm. Curves *1* are obtained by the simulation software, curves *2* are the ideal spectral curves ($K = 0$).

wavelengths of 3.2, 4, and 5 μm. As can be seen from the figure, when $K \neq 0$, the spectral curve is broadened, which means that the spectral resolution of the instrument is decreased. At the same time, the spectral broadening is increased, and the degradation of the spectral curve becomes more serious as K increases.

From the above results, it can be seen that for the low-stepped mirror, the step surface's flatness error can cause the decrease in the instrument's spectral

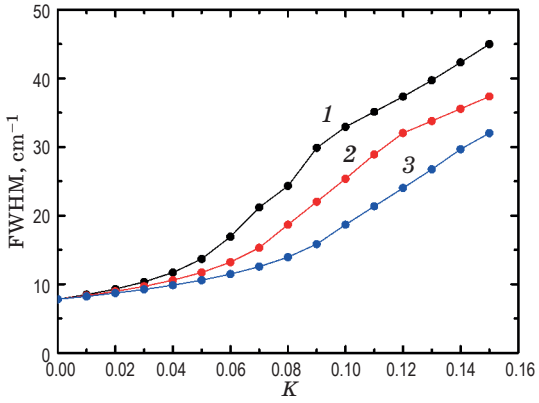

Fig. 9. Variation of FWHM with K when the wavelength is 3.2 (*1*), 4 (*2*), and 5 (*3*) μm.

resolution and the spectral line drift. Fig. 8 and Fig. 9 show that when K is equal to or less than 0.05, the peak position does not change and a high spectral resolution is obtained in the 3.2–5 μm band.

5. FABRICATION AND MEASUREMENT OF LOW-STEPPED MIRROR

5.1. Fabrication of low-stepped mirror

There has been much stress-related research, including reducing the deformation by adjusting the deposition temperature and rate [16–19]. The stair structure with 32 steps is obtained by multi-deposition, and each coating environment affects the final stress. Therefore, the stress problem of the low-stepped mirror cannot be completely solved by controlling the deposition parameters.

From the Stoney equation (11), the radius of curvature of the deformed step is proportional to the thickness of the substrate as the values of film thickness and stress remain constant

$$\sigma_f = \left(\frac{E_S}{1-V_S}\right)\frac{t_S^2}{6Rt_f}, \qquad (11)$$

where σ_f is the film stress, E_S is Young's modulus, V_S is Poisson's ratio, t_S is the thickness of the substrate, t_f is the thickness of the film and R is the radius of curvature. The radius of curvature is inversely proportional to h, so it is inversely proportional to K. Therefore, the thickness of the substrate is negatively correlated with K. In this study, the flatness error is reduced by increasing the substrate thickness.

According to the previous method, three low-stepped mirrors with 32 steps are fabricated choosing SiO_2 as thin films with 1.5-, 3-, and 5-mm substrate thickness. Meanwhile, the three mirrors are required to have the same and appropriate coating environment, including coating temperature, pressure, rate, and vacuum, to eliminate the influence of other factors. Three stepped structures with 32 steps are obtained by performing lithography and coating five times.

The flatness of the low-stepped mirrors was measured using a KLA-Tencor P-16+, as shown in Fig. 10. The maximum deviation height and K can be obtained by measuring the flatness of the low-stepped mirror. The details are shown in Table 1.

As can be seen from Table 1, the K value of the low-stepped mirror with substrate thicknesses of 1.5 and 3 mm are 0.1188 and 0.4055 respectively. From the previous section, it is discussed that the recovery spectrum curve appears in double peaks and the peak position shifted when K are 0.1188 and 0.4055 in the 3.2–5 μm working band. There is no deviation in the peak position of the recovered spectral curve with a substrate thickness of 5 mm and K value of 0.049.

The low-stepped mirror with the 5-mm substrate was deposited on a golden film as the reflective coat, as shown in Fig. 11. The height values of the

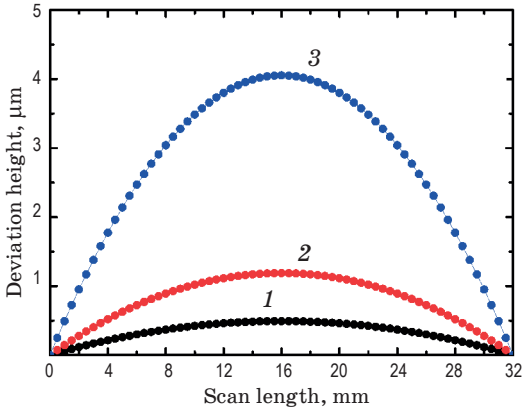

Fig. 10. Flatness test with different substrate thicknesses (*1* — 5.0, *2* — 3.0, *3* — 1.5 mm).

Fig. 11. Low-stepped mirror coated with gold reflector.

Table 1. Results of flatness test

Substrate thickness, mm	5	3	1.5
Max deviation height, μm	0.49	1.188	4.055
K	0.049	0.1188	0.4055

Table 2. Details of step height

Step height	$d_{max}/d_{max\text{-}error}$	$d_{min}/d_{min\text{-}error}$	$d_{aver}/d_{aver\text{-}error}$	Standard deviation
Values, nm	640/15	618/–7	626.9/1.9	7.4

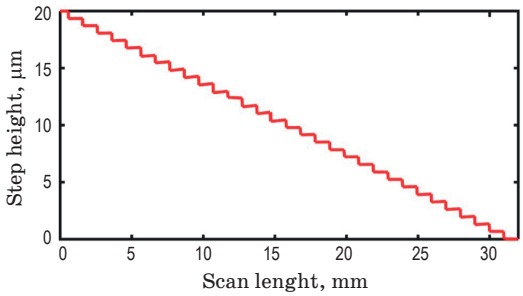

Fig. 12. Height test of low-stepped mirror with 32 steps.

low-stepped mirror were measured by a KLA-Tencor P-16+ surface profiler, as shown in Fig. 12. Details of the step height are given in Table 2. The maximum, minimum, average, and error values are included. As can be seen from Table 2, the maximum positive error is 15 nm, the maximum negative error is –7 nm and the average error is 1.9 nm. Using the Monte-Carlo method to analyse the height error [11] the results show that the height error of the low-stepped mirror satisfy the system requirements.

5.2. Experiment to measure the sample

The low-stepped mirror was incorporated into the Fourier transform infrared spectrometer, and we performed experiments to obtain the spectrum of acetonitrile liquid (CH_3CN). The prototype of the SMFTIRS is shown in Fig. 13. In this system, the step height of the tall-stepped mirror and low-stepped mirror is 20 and 0.625 μm respectively. For both cases, the step number is 32. In this experimental setup, the camera is a cooled HgCdTe middle-wave infrared detector array with 320×256 pixels, and the size of a single pixel is 30×30 μm. We obtained the interferogram recorded by the detector array.

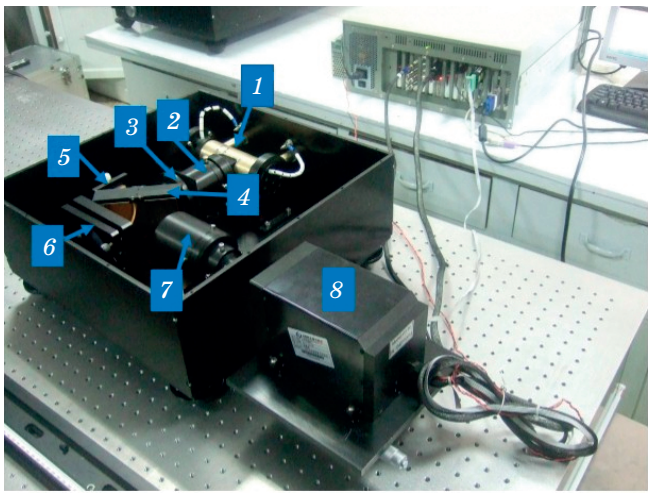

Fig. 13. Simplified configuration of the FTIRS. Light source (*1*), collimating system (*2*), sample cell (*3*), beam splitter system (*4*), tall-stepped mirror (*5*), low-stepped mirror (*6*), expansion system (*7*), and infrared detector array (*8*).

According to the working principle of the instrument, two interferograms are required, as shown in Fig. 14. The sample's absorption interferogram can be obtained by using the difference between the interferogram with and without the sample. The sample's absorption spectrum curve can be obtained by performing the Fourier transform on sample's absorption interferogram [20], as shown in Fig. 15. There is one spectral peak 2258 cm^{-1} in 3.7–4.8 μm (2702–2083 cm^{-1}) wave band. Fig. 16 is the reference spectrum of liquid acetonitrile, which is from the Coblentz Society's evaluated infrared reference spectra collection [21]. Except where noted, the spectrum data were measured on dispersive instruments, whose spectral resolution is 4cm^{-1}, and hence may differ in detail from measurements on FTIR instruments.

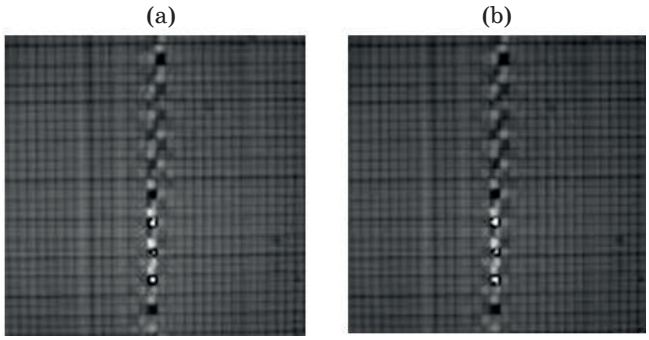

Fig. 14. Interferograms obtained before adding the sample (a) and after adding the sample (b).

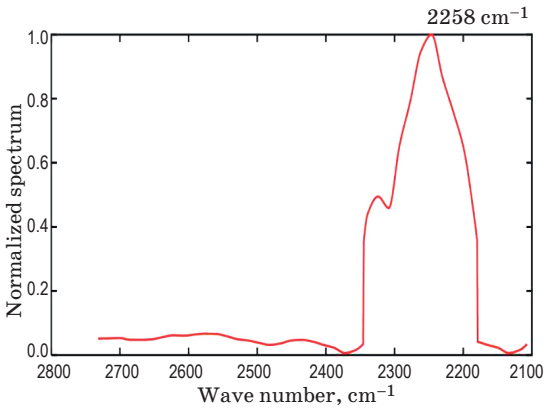

Fig. 15. Measured absorption spectrum of sample CH_3CN.

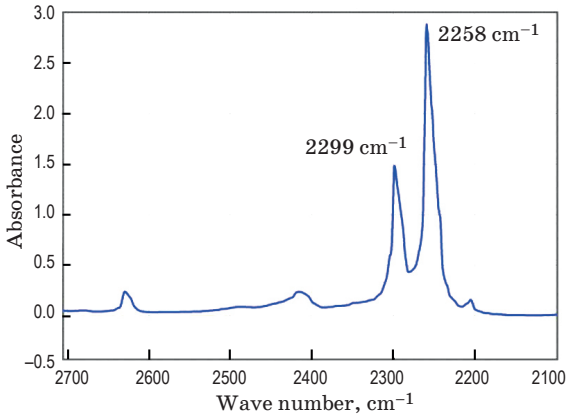

Fig. 16. Reference absorption spectrum of sample CH_3CN.

Compared Fig. 15 with Fig. 16, it can be seen that the main peak has no drift, but the spectra we obtained can't separate the main peak from the secondary peak, which is caused by the low spectral resolution. In order to obtain more accurate spectra, a further study of the instrument is needed.

6. CONCLUSION

Ideally, the step surface is presumed to be the plane in the stepped mirror, but the stress in films destroyed this imaginary. Using the method of multiple deposition to fabricate the low-stepped mirror, we can achieve a step height with high consistency and accuracy. We analysed the influence of the flatness error on the recovery spectrum using both theory and simulations. The analysis shows that the deformation of the step surface of the low-stepped mirror will lead to a degradation of the spectral curve, drift of the peak position and a broadening of the spectral curve. In this paper, we propose to increase the thickness of the substrate in order to effectively reduce the flatness error. When the substrate thickness of the low-stepped mirror is 5 mm, the peak position of the spectrum does not drift in the 3.2–5-μm band. The low-stepped mirror, which is gold-plated, was inserted in the FTIRS, and the experiment was carried out. The spectral line of a sample (CH_3CN) was obtained with an accurate peak position after processing and performing the Fourier transform of the interferogram. In order to improve the spectral resolution and reduce the noise, further research into the fabrication and analysis of low-stepped mirrors is needed.

ACKNOWLEDGMENT

This study was supported by a grant from the National Natural Science Foundation of China (NSFC) under grants 61627819, 61376122, 61575193, 6173000222 and 6172780148. Funding was also received from the Jilin Province Science and Technology Development Plan under grants 20150520101JH, 20150204072GX, 20150101049JC, and 20170204077GX, as well as the Youth Innovation Promotion Association of CAS under grant 2014193.

REFERENCES

1. *Yan M., Luo P.L., Iwakuni K., Millot G., Hänsch T.W., and Picqué N.* Mid-infrared dual-comb spectroscopy with electro-optic modulators // Light Science & Applications. 2016. V. 6. P. e17076.
2. *Wallrabe U., Solf C., Mohr J., Korvink J.G.* Miniaturized Fourier transform spectrometer for the near infrared wavelength regime incorporating an electromagnetic linear actuator // Sens. Actuators A Phys. 2005. V. 123–124. P. 459–467.
3. *Reyes D., Schildkraut E.R., Kim J., Connors R.F., Kotidis P., and Cavicchio D.J.* A novel method of creating a surface micromachined 3D optical assembly for MEMS-based miniaturized FTIR spectrometers // Proc. SPIE. 2008. V. 6888. P. 68880D.
4. *Möller K.D.* Miniaturized wavefront dividing interferometers without moving parts for field and space applications // Proc. SPIE. 1993. V. 1992. P. 130–139.
5. *Möller K.D.* Wave-front-dividing array interferometers without moving parts for real-time spectroscopy from the IR to the UV // Appl. Opt. 1995. V. 34. № 9. P. 1493–1501.
6. *Brachet F., Hébert P.J., Cansot E., Buil C., Lacan A.L., Lacan X., Courau E., Bernard F., Casteras C., Loesel J., Pierangelo C.* Static Fourier transform spectroscopy breadboards for atmospheric chemistry and climate // Proc. SPIE. 2008. V. 7100. P. 710019.
7. *Lacan A., Bréon F.M., Rosak A., Brachet F., Roucayrol L., Etcheto P., Casteras C., Salaün Y.* A static Fourier transform spectrometer for atmospheric sounding: Concept and experimental implementation // Opt. Exp. 2010. V. 18. № 8. P. 8311–8331.
8. *Ivanov E.V.* Static Fourier transform spectroscopy with enhanced resolving power // J. Opt. A: Pure Appl. Opt. 2000. V. 2. № 2. P. 519–528.
9. *Cansot E., Hébert P., Rosak A., Buil C., Benard F.* Static infrared Fourier transform interferometer (SIFTI): Benefits of phase modulation processing // Water Science & Technology Water Supply. 2007. V. 10. № 1. P. 45.
10. *Liang J.Q., Liang Z.Z., Lv J.G., Fu J.G., Zheng Y., Feng C., Wang W.B., Zhu W.B. , Yao J.S., and Zhang J.* Simulation and experiment of the static FTIR based on micro multi-step mirrors // Proc. SPIE. 2011. V. 8191. P. 819104.

11. *Chen C., Liang J.Q., Liang Z.Z., Lü J.G., Qin Y.X., Tian C., Wang W.B.* Fabrication and analysis of tall-stepped mirror for use in static Fourier transform infrared spectrometer // Opt. Laser Technol. 2015. V. 75. P. 6–12.

12. *Feng C., Liang J.Q., Liang Z.Z.* Spectrum constructing with nonuniform samples using least-squares approximation by cosine polynomials // Appl. Opt. 2011. V. 50. № 34. P. 6377–6383.

13. *Feng C., Wang B., Liang Z.Z., Liang J.Q.* Miniaturization of step mirrors in a static Fourier transform spectrometer: Theory and simulation // JOSA B. 2011. V. 28. № 28. P 128–133.

14. *Lv J.G., Liang J.Q., Liang Z.Z., Qin Y.X., Tian C., and Wang W.B.* Design and manufacture of micro interference system in spatial modulation Fourier transform spectrometer // Key Engineering Materials. 2013. V. 562–565. P. 973–978.

15. *Nix W.D., Clemens B.M.* Crystallite coalescence: A mechanism for intrinsic tensile stresses in thin films // J. Materials Research. 1999. V. 14. № 8. P. 3467–3473.

16. *Schriever C., Bohley C., Schilling J., Wehrspohn R.B.* Strained silicon photonics // Materials. 2012. V. 5. № 5. P. 889–908.

17. *Cha S., Lee H., Lee W., Kim H.* Platinum bottom electrodes formed by electron-beam evaporation for high-dielectric thin films // Japanese J. Appl. Phys. 2014. V. 34. № 9. P. 5220–5223.

18. *Ha P.C.T., Mckenzie D.R., Doyle D., Mcculloch D.G., Wuhrer R.* Multilayer structure, stress reduction and annealing of carbon film // MRS Proc. 2003. V. 791. P. Q5.30.

19. *Jerman M., Mergel D.* Post-heating of SiO_2 films for optical coatings // Thin Solid Films. 2008. V. 516. № 23. P. 8749–8751.

20. *Gao J.H., Liang Z.Z., Liang J.Q., Wang W.B., Lv J.G., Qin Y.X.* Spectrum reconstruction of static step-mirror based Fourier transform spectrometer // Appl. Spectr. 2017. V. 71. № 6. P. 1348.

21. https://webbook.nist.gov/cgi/cbook.cgi?ID=C75058&Units=SI&Type=IR-SPEC&Index=2#Refs